

<https://doi.org/10.1038/s41612-024-00806-y>

Synchronous decadal climate variability in the tropical Central Pacific and tropical South Atlantic



Chao Liu ¹✉, Soon-Il An ^{1,2,3}✉, Soong-Ki Kim ¹, Malte F. Stuecker ⁴, Wenjun Zhang ^{5,6}, Fei-Fei Jin ⁷, Jae-Heung Park ⁸, Leishan Jiang ^{5,6}, Aoyun Xue ⁹, Xin Geng ^{5,6}, Hyo-Jin Park ², Young-Min Yang ¹⁰ & Jong-Seong Kug ⁸

Pantropical climate interactions across ocean basins operate on a wide range of timescales and can improve the accuracy of climate predictions. Here, we show in observations that Central Pacific (CP) El Niño-like sea surface temperature (SST) anomalies have coevolved with tropical South Atlantic SST anomalies on a quasi-decadal (~10-year) timescale over the past seven decades. During the austral autumn–winter season, decadal warm SSTs in the tropical CP effectively induce tropical SST cooling in the South Atlantic, mainly by strengthening the South Atlantic subtropical anticyclone via an extratropical atmospheric wave teleconnection in the southern hemisphere. Partially coupled pacemaker simulations corroborate the observational findings, indicating that tropical CP decadal SSTs play a primary pacing role, while Atlantic feedback is of secondary importance throughout the study period. Our results suggest that the tropical CP could be an important source of decadal predictability for tropical South Atlantic SST and the surrounding climate.

Pantropical climate interactions refer to the coupling of climate variability across three ocean basins, with the potential to improve the accuracy of climate predictions compared to using forecast information from a single basin^{1–3}. In particular, the interaction between the tropical Pacific and Atlantic Ocean basins has received considerable attention^{4–6} over the past decade. In both ocean basins, the multiple timescales characteristic of climate variability, ranging from seasonal to decadal, require a better understanding of the potentially timescale-dependent linkages and associated physical processes. This improved knowledge can benefit seasonal to multiannual climate prediction⁷.

On interannual timescales (<7 years), tropical Pacific climate variability is dominated by the El Niño Southern Oscillation (ENSO), the strongest air–sea coupled variability in the climate system⁸. Its remote effects on the tropical Atlantic are well established. For example, during the boreal spring of the El Niño decay phase, tropical North Atlantic sea surface temperature (SST) anomalies⁹ usually show pronounced warming responses under the influence of several tropical and extratropical

atmospheric teleconnection pathways^{5,10–13}. Interestingly, however, the influence of ENSO on equatorial Atlantic SST (i.e., Atlantic Niño¹⁴) appears to be much smaller, with no significant concurrent or lagged linear relationship observed¹⁵. This has been attributed to the competing effects of thermodynamic atmospheric warming and wind-induced dynamic ocean cooling associated with the ENSO¹⁶, the delayed negative impact of North Atlantic SST¹⁷, and the complexity of Pacific ENSO events¹⁸. Conversely, tropical Atlantic SST anomalies may also influence the ENSO. For example, during the boreal spring and summer seasons, equatorial and tropical North Atlantic SST anomalies tend to be associated with opposite tropical Pacific SST anomalies, especially in recent decades of observations, and have thus been proposed as favorable precursors of subsequent ENSO events^{19–23}. An alternative, competing hypothesis is that these antecedent tropical Atlantic SST signals are mostly ENSO teleconnection remnants within the complex ENSO cycles⁴, or seasonally modulated ENSO responses^{6,24} with limited feedback to the Pacific.

¹Irreversible Climate Change Research Center, Yonsei University, Seoul, Republic of Korea. ²Department of Atmospheric Sciences, Yonsei University, Seoul, Republic of Korea.

³Division of Environmental Science and Engineering, Pohang University of Science and Technology (POSTECH), Pohang, Republic of Korea. ⁴Department of Oceanography & International Pacific Research Center (IPRC), School of Ocean and Earth Science and Technology (SOEST), University of Hawai'i at Mānoa, Honolulu, HI, USA. ⁵CIC-FEMD/ILCEC, Key Laboratory of Meteorological Disaster of Ministry of Education (KLME), Nanjing University of Information Science and Technology (NUIST), Nanjing, China.

⁶School of Atmospheric Sciences, Nanjing University of Information Science and Technology (NUIST), Nanjing, China. ⁷Department of Atmospheric Sciences, School of Ocean and Earth Science and Technology (SOEST), University of Hawai'i at Mānoa, Honolulu, HI, USA. ⁸School of Earth and Environmental Sciences, Seoul National University, Seoul, South Korea. ⁹Bren School of Environmental Science and Management, University of California, Santa Barbara, Santa Barbara, CA, USA. ¹⁰Department of Environment & Energy/School of Civil, Environmental, Resources and Energy Engineering/Soil Environment Research Center, Jeonbuk National University, Jeonju-si, Republic of Korea.

✉e-mail: liuc@yonsei.ac.kr; sian@yonsei.ac.kr

In addition, many studies have identified pronounced quasi-decadal (~10 years) variability in both the tropical Pacific and the Atlantic, and have discussed the physical processes within each basin. However, compared to the interannual timescale, their linkages on this quasi-decadal timescale have not been well recognized. Specifically, there is a distinct Central Pacific (CP) ENSO-like quasi-decadal variability in the tropical Pacific^{25,26}, which is an important constitute of the multifaceted statistical decadal modes of the Pacific decadal oscillation^{27,28} or interdecadal Pacific oscillation²⁹ and accounts for a substantial part of their decadal variability^{25,30}. Spatially, it resembles the SST structure of the North Pacific meridional mode^{31–33} and is accompanied by extratropical North Pacific oscillation-like atmospheric circulation anomalies³⁴, which drive decadal variability in the North Pacific^{35,36} and provide positive feedback to the tropical Pacific SST through the seasonal footprint mechanism³¹. Although elusive, its preferred quasi-decadal timescale has been suggested to originate primarily from ocean dynamics^{37,38}, including decadal oceanic off-equatorial Rossby wave adjustments³⁹, decadal variations in the strength of the shallow upper-ocean overturning circulation^{40,41}, and/or the nonlinear rectification associated with the bursting of strong ENSO events^{26,42}, etc. By triggering the tropical central western Pacific deep convection, it strongly influences the weather and climate around the Pacific rim, including the East Asian rainfall⁴³, the western Pacific tropical cyclone⁴⁴, the North American precipitation⁴⁵, and the Antarctic climate⁴⁶ in the southern hemisphere.

In the tropical Atlantic, a similar quasi-decadal (~13 years) timescale variability in the Atlantic meridional mode has been identified in early observational reanalysis, which affects regional climate^{47,48} and could arise from the unstable thermodynamic ocean-atmosphere interactions (i.e., wind-evaporation-SST feedback)⁴⁹. Another study⁵⁰ also recognized the thermodynamic feedback in determining the growth and spatially dipolar SST structure, but further argued that forcing from or interaction with the extratropical North Atlantic needs to be invoked to explain the preferred quasi-decadal timescales, as the tropical Atlantic alone does not favor any particular timescale. In this context, the tropical Atlantic meridional dipole may be viewed as part of a coherent Pan-Atlantic decadal oscillation that also includes the decadal variability of the North Atlantic Oscillation^{51–53}. Meanwhile, other early studies^{54,55} have identified a similar timescale decadal variability with a dominant period of about 20 years in the South Atlantic that manifests as a north-south dipole structure in the SST field (i.e., the South Atlantic Subtropical Dipole^{56,57}, SASD; or South Atlantic Ocean Dipole, SAOD^{58,59}) coupled with a sea level pressure monopole that describes the strength of the South Atlantic Subtropical Anticyclone⁶⁰. Particularly, the northern lobe of this South Atlantic decadal SST variability is oriented towards the tropical southeast Atlantic, indicating its contribution to the tropical Atlantic decadal variability in the Atlantic Niño and Benguela Niño regions^{61,62}. It is further suggested that this South Atlantic decadal SST dipole may be a regional aspect of the global interdecadal variability⁶³, but no detailed explanations involving teleconnection physics and preferred timescale mechanisms are presented in this early work.

Given the similar quasi-decadal timescale variability in both the tropical Pacific and the Atlantic, it is reasonable to speculate about their possible connections. Some evidence of Pan-Pacific-Atlantic connectivity, mostly in the southern hemisphere, is emerging from interannual study results. For example, while previous studies suggested largely independent variability between ENSO and SAOD^{55,58}, a recent study⁶⁴ found that interannual ENSO influences, although weakly significant, can somehow be detected in the upwelling SST of the Benguela Current in the austral summer via mediating the key atmospheric circulation system of the South Atlantic Subtropical Anticyclone⁶⁵. Rodrigues et al. (2015)⁶⁶ found that compared to the Eastern Pacific ENSO, the CP ENSO exerts a stronger influence on the SAOD on interannual timescales during its peak phase (i.e., austral summer) by more effectively exciting the Pacific-South American wave train that modifies the South Atlantic Subtropical Anticyclone. Focusing on the Atlantic Niño region, Jiang et al. (2023)⁶⁷ argued for asymmetric modulation effects of El Niño and La Niña phases on equatorial Atlantic SST anomalies, with the asymmetric atmospheric heating mainly located in the tropical CP

to the Maritime Continent. Given the pronounced quasi-decadal variability in the tropical CP and the key role of the subtropical anticyclone circulation system in controlling the South Atlantic decadal SST variability^{54,55} and its tropical extensions, these results indicate that some decadal linkages might exist between the CP and tropical Atlantic SSTs. Furthermore, Zhao and Capotondi (2024)⁶⁸ investigated the Pacific-Atlantic interactions using an observational-trained linear inverse model and found that decoupling of the Atlantic from the Pacific enhances the decadal variance of the tropical CP, suggesting that the overall Pan-Pacific-Atlantic interaction may dampen CP ENSO-like decadal variability.

Despite the above evidence, the overall picture of the two-basin connection on this quasi-decadal timescale remains largely unclear. Previous studies of quasi-decadal variability in the tropical Atlantic are mostly based on early observational reanalysis^{49,54,55,63}, making their results less certain in the context of modern data. To fill this important knowledge gap, we revisit this topic and focus on the two-basin interactions with the following specific questions: (1) To what temporal and spatial extent are the quasi-decadal SSTs of the tropical Pacific and the tropical Atlantic coupled? That is, what is the spatial pattern and temporal evolution of coupled interbasin variability on this quasi-decadal timescale? Does the tropical North and South Atlantic SST anomaly show a similar decadal connection to the tropical Pacific or not? How strong is the Pacific-Atlantic connection and does it show any seasonal preferences? (2) How are the two basins coupled? That is, what are the key processes that link the two ocean basins on quasi-decadal timescales? Is the Pan-Pacific-Atlantic decadal covariability mainly driven by one basin or by mutual interactions? (3) How to understand the preferred quasi-decadal timescale in the tropical Atlantic?

In this paper, using modern ocean-atmosphere reanalysis datasets from the last seven decades (1951–2022) and idealized coupled pacemaker experiments, we find a robust synchronization relationship throughout our study period between the decadal climate in the tropical CP and the tropical South Atlantic in austral autumn-winter seasons. For the tropical North Atlantic SST anomaly, its decadal connection with the Pacific is much weaker and mostly statistically insignificant. Such a Pan-Pacific-South Atlantic quasi-decadal covariability is primarily bridged by the Pacific-South American wave train in the extratropical southern hemisphere, while the feedback from the tropical Atlantic decadal SST to the Pacific is of secondary importance. We suggest that the preferred quasi-decadal timescale of the tropical Atlantic SST is, at least in part, externally controlled by the remote tropical Pacific.

Results

Decadal SST energy map and Pacific-Atlantic synchronization

Figure 1 shows the main active region of the tropical quasi-decadal SST variability, indicated by the standard deviation and variance ratio of the decadal SST anomaly in its dominant frequency band of 8–16 years (see power spectrum results in Fig. 2). Results are not sensitive to the choice of filter windows, such as 8–20 years²⁶ or 10–15 years⁴⁵ as used in previous studies. Here we divide the annual data into two seasons: March–August (MAMJJA) and September–February (SONDJF) to account for the seasonality of tropical Atlantic SST variability, which is more pronounced in the boreal spring-summer season^{14,58,69}. Consistent with previous studies^{25,26,35}, the quasi-decadal SST variability is more dominant in the tropical Pacific than in the other two basins, showing a broad CP ENSO-like structure with the equatorial CP SST magnitude around 0.3–0.4 °C throughout the year and accounting for 15–25% of the total SST variability (Fig. 1). The Atlantic counterpart is comparatively weaker, showing a dipole-like decadal SST signal of about 0.1–0.2 °C mainly in the southern hemisphere during the MAMJJA season and accounting for ~15% of the SST variance (Fig. 1a). In particular, the maximum decadal SST standard deviation around the Benguela Niño region and the coastal regions of São Paulo is reminiscent of the South Atlantic subtropical dipole^{54,55,57}, which is coupled to the South Atlantic subtropical anticyclone and shows pronounced decadal variability. In contrast, the quasi-decadal SST variability in the tropical North Atlantic or in the SONDJF season (Fig. 1b) is much

Fig. 1 | Quasi-decadal SST variance maps. Maps of the decadal SST standard deviation (shading, unit: K) on an 8–16-year frequency band and its variance ratio (contours, units: %) relative to the raw SST anomaly during the **a** March to August (MAMJJA) and **b** September to February (SONDJF) seasons for the period 1951–2022. The blue dashed boxes enclose the Niño4 (160° E–150° W, 5° S–5° N) and tropical South Atlantic (40° W–10° E, 15° S–0° N) regions.

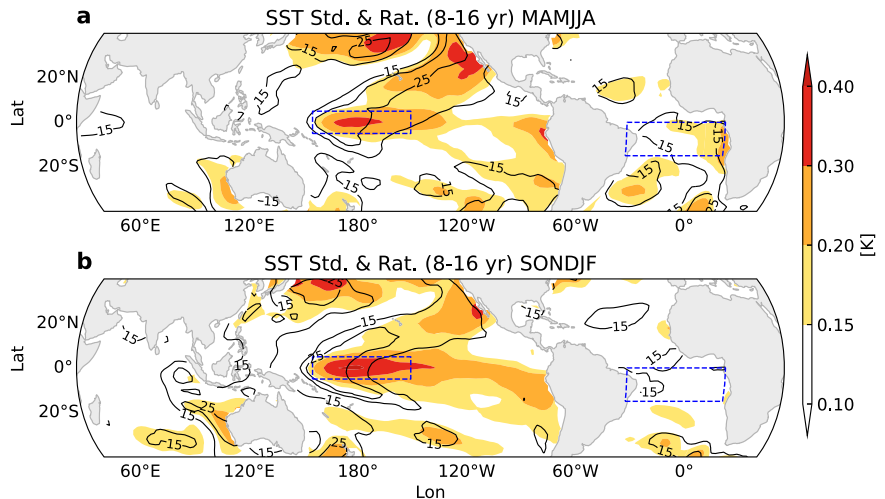
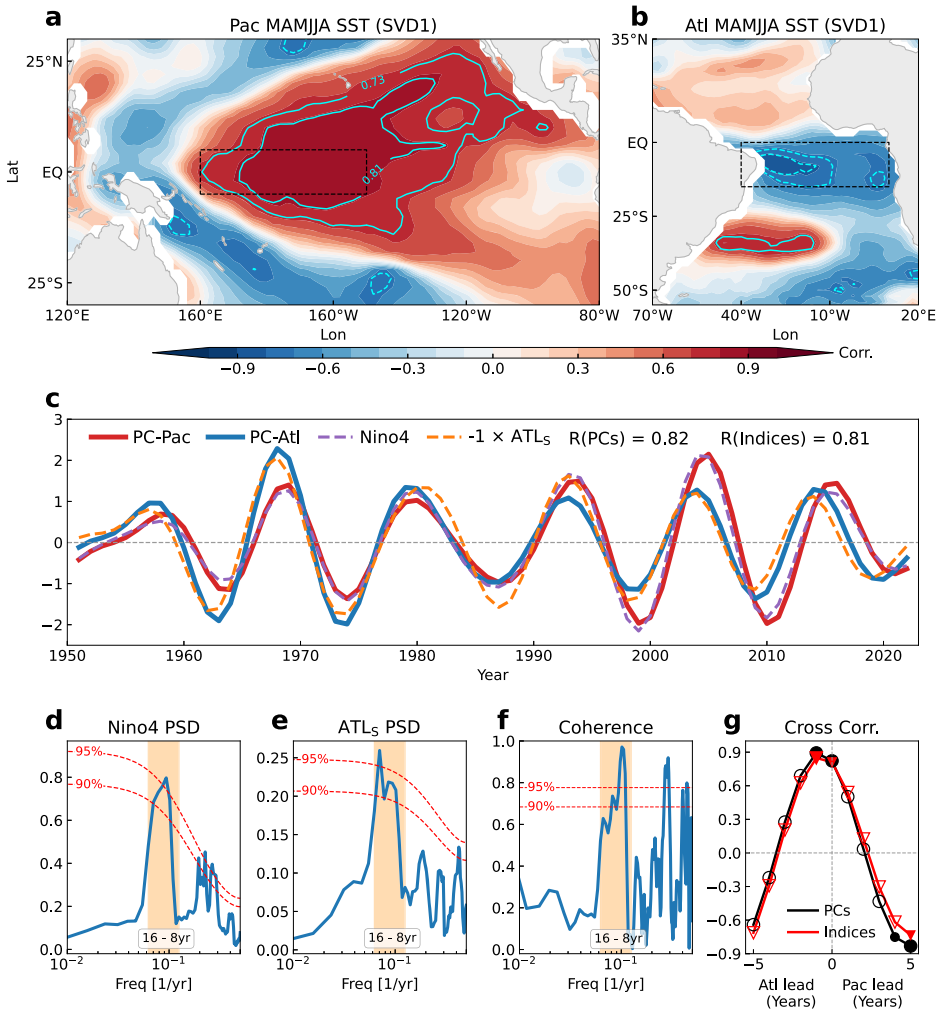


Fig. 2 | Synchronization of CP and South Atlantic decadal SSTs. Heterogeneous correlation patterns (shading) for the leading pair of the MCA mode between the tropical Pacific (120° E–80° W, 30° S–30° N) and **b** the Atlantic (70° W–20° E, 55° S–35° N) 8–16-year bandpass filtered MAMJJA SST anomalies. The cyan contours denote isolines of ± 0.73 and 0.81 , corresponding to the 90% and 95% confidence levels with approximately 6 decadal cycles. **c** Normalized principal components (PCs) for the Pacific (red) and Atlantic (blue) MCA SST modes. The normalized decadal Niño4 (purple; 160° E–150° W, 5° S–5° N) and sign-reversed tropical South Atlantic (ATL_S; orange; 40° W–10° E, 15° S–0° N) SST indices are also superimposed, with areas enclosed by black dashed boxes in **(a, b)**. Multi-taper (tapers = 3) power spectra of the MAMJJA raw **d** Niño4, **e** sign-reversed ATL_S SST index, and **f** their coherence spectrum. The 90% and 95% confidence levels based on an AR(1) null hypothesis are shown as red dashed lines, while the orange shading denotes the quasi-decadal timescale of 8–16 years. **g** Cross-correlation coefficients as a function of the year between the pair MCA PCs (black line) and SST indices (red line). Positive leads indicate that the Pacific signal leads the Atlantic signal and vice versa. Large and small filled dots mark correlations above the 90% and 95% confidence levels.



weaker and less organized. Thus, in the following analyses, we will primarily focus on the decadal SST variability during the MAMJJA season in the tropical South Atlantic, and as will be verified below, this season and region also show the strongest Pan-Pacific–Atlantic quasi-decadal connection.

To extract the decadal covariability between two ocean basins, we performed a maximum covariance analysis (Fig. 2a–c) using 8–16 years bandpass filtered MAMJJA SST anomalies in the tropical Pacific (120°

E–80° W, 30° S–30° N) and Atlantic (70° W–20° E, 55° S–35° N). For the first MCA mode (expvar 55.1%), the heterogeneous correlation pattern of the Pacific SST shows a well-known CP ENSO-like structure, with an equatorial CP maximum extending towards the northeastern subtropical Pacific (Fig. 2a), while the Atlantic counterpart (Fig. 2b) shows an SASD/SAOD-like^{54,57,58} meridional dipole structure mainly in the southern hemisphere, with prominent negative correlations in the tropical South Atlantic and a

positive correlation lobe near the São Paulo coastal region. Interestingly, the heterogeneous correlation in the tropical North Atlantic (Fig. 2b) is only weakly positive, indicating a small contribution of local SST to the Atlantic leading principal component (PC) variability. Such a weak decadal connection between the tropical CP and the tropical North Atlantic is further evidenced by the second MCA mode (expvar 15.8%; Supplementary Fig. 1), which shows strong loading in the tropical North Atlantic but almost muted signals in the tropical CP. In other words, the highly correlated leading PC time series ($r = 0.82$, $p = 0.05$; Fig. 2c) essentially reflects a synchronization relationship between the CP ENSO-like and the South Atlantic decadal SST over the past seven decades. Consistent MCA results are also obtained in another SST reanalysis product, but with a zonal shift of the tropical South Atlantic maximum correlation center in its first MCA mode (Supplementary Figs. 2 and 3).

To validate our results, we also analyzed area-averaged SST indices in the Niño4 (160° E–150° W, 5° S–5° N) and tropical South Atlantic (40° W–10° E, 15° S–0°) regions. The power and coherence spectra of both unfiltered indices all show a clear quasi-decadal peak (8–16 years) above the 95% confidence level (Fig. 2d–f and Supplementary Fig. 2d–f), corroborating our previously identified quasi-decadal variability and coherent inter-basin decadal relationship. Moreover, their quasi-decadal components show almost identical decadal variations as the leading pair of PCs (Fig. 2c and

Supplementary Fig. 2c), suggesting that they well represent the quasi-decadal variability in each basin. The cross-correlation results (Fig. 2g and Supplementary Fig. 2g) also support a decadal Pan-Pacific–Atlantic synchronization paradigm, but with the South Atlantic variability slightly leading the Pacific by one year.

We note that on our target quasi-decadal timescale (i.e., 8–16 years), such a small statistical phase lag does not necessarily imply a physical causality from the Atlantic to the Pacific, since the Pacific decadal SST is already evident to drive atmospheric teleconnections a year before its peak, but is more likely due to a small temporal difference in tropical and extra-tropical teleconnections that oppositely influence the tropical South Atlantic SST (see next section). Furthermore, our choice of MCA analysis season and domain can be additionally supported by the correlation maps between the annual-mean decadal Niño4 index and the global decadal SSTs in four seasons, which show that the strongest Pan-Pacific–Atlantic teleconnection occurs mainly in the tropical South Atlantic during the boreal spring and summer seasons (Supplementary Fig. 4).

Decadal evolution of ocean-atmosphere conditions

To understand the physical processes driving the inter-basin decadal covariability, Fig. 3 shows lead-lag regressed maps of key ocean-atmosphere surface variables, including SST, outgoing longwave radiation as a proxy for

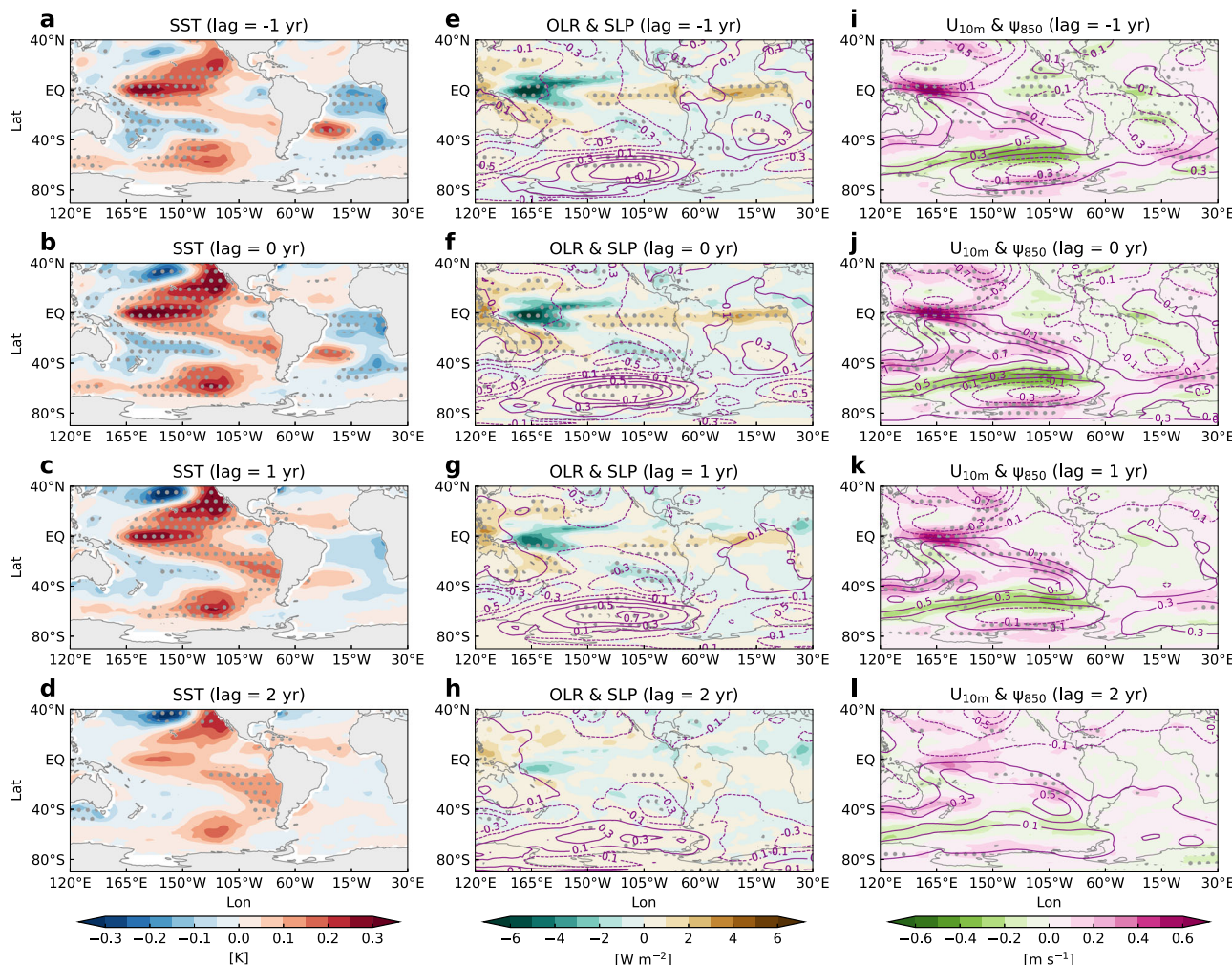


Fig. 3 | Evolution of surface ocean-atmosphere conditions for decadal inter-basin linkages. **a–d** Regression maps of SST (unit: K) onto normalized 8–16-year bandpass filtered MAMJJJA Niño4 index at different time lags. A positive lag indicates that the index leads the physical field and vice versa. **e–h** as (a–d), but for outgoing longwave radiation (OLR; shading, positive upward, unit: W m^{-2}) and sea level pressure anomalies (contours, unit: hPa). **i–l** same as (a–d), but for 10 m wind speed

(shading, unit: m s^{-1}) and 850 hPa stream function anomalies (contours, unit: $10^6 \text{ m}^2 \text{s}^{-1}$). The positive values of the stream function represent anticyclonic circulation in the northern hemisphere and cyclonic circulation in the southern hemisphere, and vice versa. Regression coefficients exceeding the 90% confidence level based on a two-tailed Student's *t*-test are stippled.

deep convection, sea level pressure, 10 m wind speed, and the 850 hPa stream function, onto the normalized decadal Niño4 index. The results are insensitive to the choice of SST index, as both the Pacific and Atlantic SST indices have nearly identical decadal components (Fig. 2c, g; $R \sim 0.9$).

One year before the Pacific SST peak (i.e., lag = -1 year), both the CP ENSO-like and the South Atlantic SST are already apparent and statistically significant (Fig. 3a). Interestingly, there is almost no SST signal observed in the tropical North Atlantic, consistent with the previous MCA results (Fig. 2a, b). The warm tropical CP SST (Fig. 3a) induces local deep convection and broad negative sea level pressure anomalies (Fig. 3e), which also manifest as a pair of low-level cyclonic circulation anomalies with negative and positive 850 hPa stream function anomalies north and south of the equator (contours in Fig. 3i). The associated equatorial CP surface westerlies (shaded in Fig. 3i) extend southeast and northeast toward subtropical Pacific regions, leading to positive SST anomaly via equatorial Bjerknes feedback and off-equatorial wind-driven latent heat flux changes^{26,33}. Similarly, the negative South Atlantic SST anomaly (Fig. 3a) is accompanied by a local positive sea level pressure anomaly (contours in Fig. 3e) and a pair of low-level anticyclonic circulations straddling the equator (contours in Fig. 3i). In particular, the more evident South Atlantic subtropical anticyclone (contours in Fig. 3e, i), which indicates a strengthened South Atlantic subtropical high⁶⁰, is oriented northwest-southeast, parallel to the orientation of the climatological South Atlantic convergence zone⁷⁰, suggesting a potential anchoring effect by this moisture-rich system. The associated large-scale surface easterlies in the South Atlantic (shaded in Fig. 3i) play similar roles to those in the tropical Pacific, cooling equatorial and off-equatorial SSTs mainly through oceanic thermocline feedback (TF) and the wind-driven latent heat flux changes, respectively (see “Methods”; Supplementary Fig. 5).

One year later (i.e., lag = 0 year), the Pacific SST pattern intensifies to its peak phase, while the Atlantic SST pattern begins to weaken slightly but remains statistically significant (Fig. 3b). Such an early decay of the Atlantic SST leads to a statistical one-year phase lag between the two ocean basins (Fig. 2g) and is mainly due to the stronger ENSO SST and the associated thermodynamic damping effect of the atmospheric warm Kelvin wave teleconnection (see next section). However, the overall similarity of ocean-atmosphere conditions between these two lags (i.e., lag = -1 years, 0 years; Fig. 3a, b, e, f, i, j) suggests that persistent teleconnection pathways are at work, and thus the small phase lag does not indicate physical causality. At longer lags, the SST decays in both basins, with the equatorial Pacific SST center (Fig. 3c, d) gradually moving eastward and poleward into the subtropical regions due to slow oceanic adjustment processes, while the South Atlantic SST shows locally rapid decay with no obvious propagation features. The atmospheric response is consistently reduced along with these attenuated SSTs (Fig. 3g, h, k, l).

Considering a synchronous Pan-Pacific-Atlantic decadal connection, we present the above results for time lags from -1 years to 2 years. To complete a full $\pm\pi/2$ phase evolution of a dominant quasi-decadal periodicity of 12 years (i.e., ± 3 years), we also supplement these physical quantities at early (i.e., lag = -3 years and -2 years) and late (lag = 3 years) lags (Supplementary Fig. 6). At these lags, most of the physical quantities become statistically insignificant, with less clear evidence to resolve the inter-basin causality. For example, at a lag of -2 years (Supplementary Figs. 6b, e), the tropical CP SST and local OLR are below and above the 90% confidence level, respectively, while the opposite situation of broadly significant SST and insignificant OLR is observed in the tropical South Atlantic. In other words, the weak decadal signal-to-noise ratio and limited observed decadal samples make it difficult to strictly distinguish the first trigger of the decadal interbasin connection during the onset phase.

The phase evolution of the Pan-tropical Pacific-Atlantic decadal connection depicted by the above cross-correlation analysis can also be verified by another signal analysis approach, namely, multitaper frequency-domain singular value decomposition (MTM-SVD)⁷¹. This method has been widely used in previous studies^{26,72,73} to detect the time-scale dependent coupling between different physical quantities of interest and can avoid the a priori selection of the bandpass filter frequency band. Using the MAMJJA

raw SST anomalies and its combinations of several key atmospheric fields covering most of the Pacific and Atlantic Oceans (120°E – 180°E , 60°S – 60°N), the diagnostic metric of the local fractional variance spectra show significant narrow-band interannual and quasi-decadal (8–16 years) peaks (Supplementary Fig. 7). In particular, the reconstructed typical phase evolution on a decadal (10.67 year) timescale (Supplementary Fig. 8) is highly consistent with the MCA result (Fig. 2) and Niño4-based lead-lag analyses (Fig. 3), showing a tightly synchronous decadal coevolution between the tropical CP and the tropical South Atlantic SST. Moreover, we found that the Pacific deep convection is stronger and established earlier than the tropical Atlantic counterpart (Supplementary Fig. 8j, k), suggesting a potentially more dominant role of the Pacific. In contrast, on a typical interannual timescale (3.57 years; Supplementary Fig. 9), equatorial Atlantic SST anomaly coevolves with Eastern Pacific El Niño only during its development phase (Supplementary Fig. 9b–d). During the peak and decay phases of El Niño (Supplementary Fig. 9e–i), the equatorial Atlantic SST anomaly is largely muted, but the tropical North Atlantic and subtropical South Atlantic SST anomalies gradually evolve into pronounced warming responses. These results are consistent with the previously identified ENSO teleconnection to the tropical North Atlantic⁵ and subtropical South Atlantic⁷⁰, and an overall fragile interannual relationship between El Niño and equatorial Atlantic SST¹⁶. The distinct interannual and decadal inter-basin connections may be related to the time-scale dependent Pacific SST patterns and intensities, which drive different tropical precipitation responses and remote atmospheric teleconnections.

Roles of tropical and extratropical teleconnection pathways

The wave-train-like subtropical low-level circulations (Fig. 3 and Supplementary Fig. 8) suggest a potential role for extratropical atmospheric teleconnections in synchronizing the decadal climate of the two basins. In response to the CP ENSO-like SST forcing (Fig. 3a–c), the equatorially enhanced deep convection excites upper-level atmospheric Rossby wave perturbations, emanating wave fluxes that propagate poleward and southeastward to the southern tip of South America and then deflect northeastward into the Atlantic tropics (Fig. 4a–c). A similar extratropical teleconnection pathway is also evident in the MTM-SVD results (Supplementary Fig. 8) and has been invoked in previous studies to link the tropical CP SST anomaly to the Antarctic^{74,75} or South Atlantic climate^{64,66} on interannual timescales. Such Pacific-Atlantic energy dispersion influences the key subtropical low-level anticyclone system, cooling tropical South Atlantic SSTs by low-level easterlies in this northern flank. The resulting negative SST responses can drive low-level easterly winds and anticyclonic Rossby wave circulations according to Gill theory⁷⁶, and thus potentially provide positive feedback to intensify the anticyclonic circulations into the observed pattern. As the Pacific SST anomalies weaken and move eastward, this atmospheric bridge is disrupted (Fig. 4d), and the Atlantic SST anomalies disappear (Fig. 3d).

In addition to extratropical atmospheric Rossby wave teleconnections, the tropical teleconnection pathway is also evident. One year before the Pacific SST peaks (i.e., lag = -1 year), equatorial Central-western Pacific deep convection releases latent heat and warms the tropical tropospheric air temperature (TT), manifesting as a coupled Kelvin-Rossby wave mainly in the tropical Pacific, with no signal in the tropical Atlantic (Fig. 4e). The Pacific SST reaches its peak phase one year later (i.e., lag = 0 year), driving a stronger TT signal that penetrates the tropical Atlantic (Fig. 4f). Such a remote TT response has a thermodynamic warming effect on the tropical Atlantic SST by stabilizing the atmosphere⁷⁷, thereby weakening the negative SST anomalies in the tropical South Atlantic, but slightly strengthening the positive SST anomalies in the tropical North Atlantic (Fig. 3b–d). This slightly damped tropical South Atlantic decadal SST during the Pacific SST peak phase is responsible for the statistical one-year phase differences between the two basins, as we have shown and discussed before.

During the decay phase (i.e., lag = 1, 2 years), the Pacific SST gradually moves poleward and eastward (Fig. 3c, d), which consistently promotes the eastward propagation of the atmospheric warm TT signal (Fig. 4g, h) and

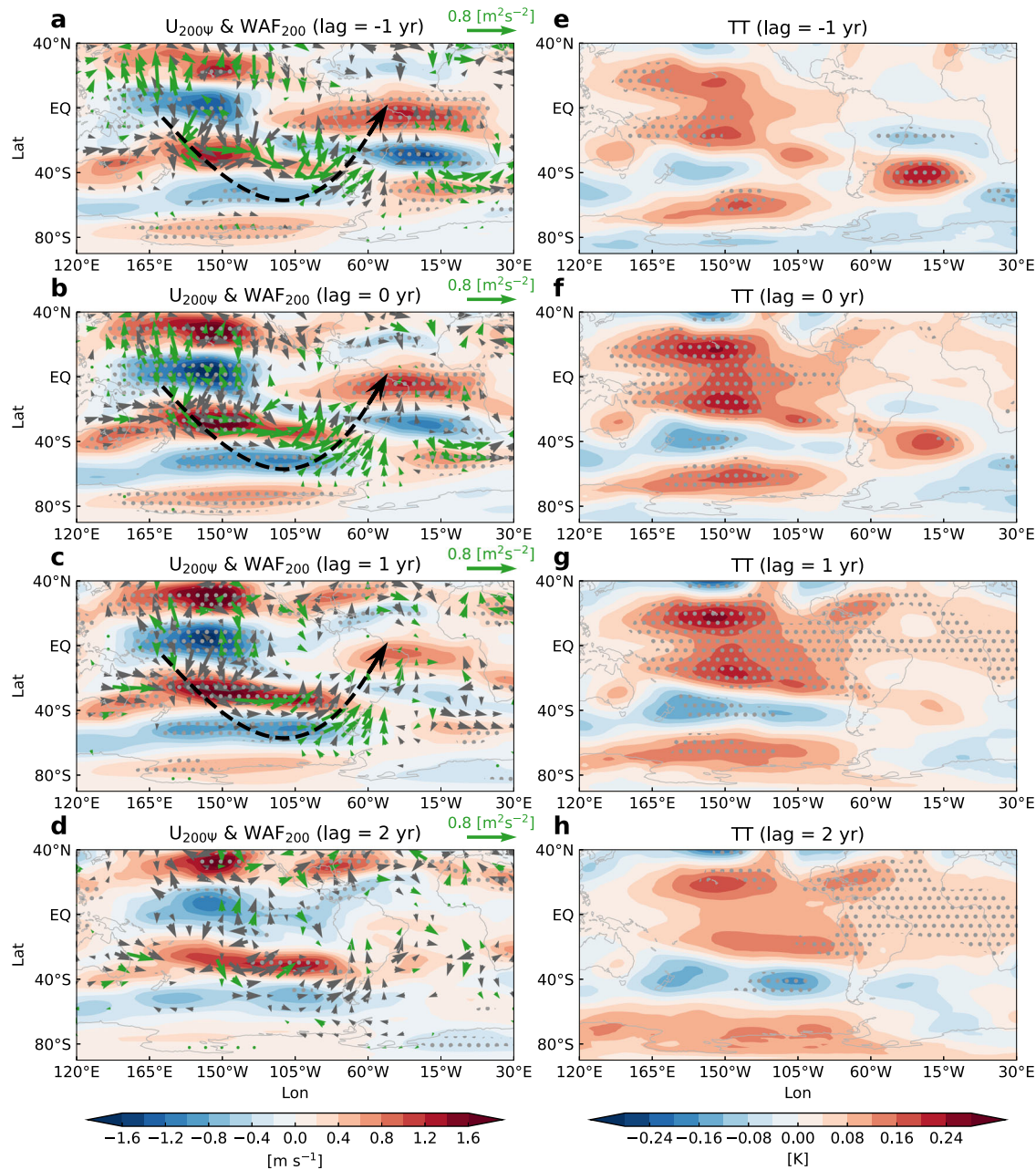


Fig. 4 | Competing extratropical and tropical teleconnection pathways.

a–d Regression maps of the 200 hPa rotational zonal wind (shading, unit: m s^{-1}) and wave activity flux (vectors, unit: $\text{m}^2 \text{s}^{-2}$) onto the normalized 8–16-year bandpass filtered MAMJJA Niño4 index at different time lags. Positive lag indicates that the index leads the physical field and vice versa. **e–h** same as (a–d), but for TT anomalies

(unit: K) vertically averaged between 850 hPa and 200 hPa. Black dashed arrows in (a–c) illustrate the southern hemisphere extratropical teleconnection pathway. Stippled shading and green vectors indicate regression coefficients exceeding the 90% confidence level based on a two-tailed Student's *t*-test.

increases the thermodynamic damping effect on the tropical South Atlantic SST. Meanwhile, as the Pacific TT signal enters the Atlantic sector, although the atmospheric Kelvin wave and associated surface easterlies on its far eastern side may also contribute to cooling the Atlantic SST, its effect may be too weak to counteract the thermodynamic TT damping effects given the rapid decay of the South Atlantic SST (Fig. 3c, d).

We note here that the coupled nature of the observations makes it difficult to directly resolve TT-related thermodynamic feedback processes through the surface energy budget (Supplementary Fig. 5)⁷, which already includes adjusted Atlantic SST signals, and to cleanly separate tropical Kelvin wave and extratropical Rossby wave teleconnections. Nevertheless, the slightly delayed arrival of the tropical warm TT signal relative to the extratropical wave teleconnection suggests a possible first trigger by the

latter, while their subsequent competition weakens the Atlantic SST response and leads to the intriguing one-year SST phase difference between the two basins. Apart from the atmospheric wave teleconnections, we also examined the role of the zonal Walker circulation and found that it exhibits a low-level descending branch centered around Recife, accompanied by weak and statistically insignificant low-level divergent westerlies in the tropical Atlantic, suggesting a minor competing effect with the wave-induced easterlies (Supplementary Fig. 10).

Pacific–Atlantic decadal connection in model experiments

To disentangle the respective roles of Pacific and Atlantic SST in the inter-basin connections through atmospheric teleconnections, we conducted a series of sensitivity experiments using the Geophysical Fluid Dynamics

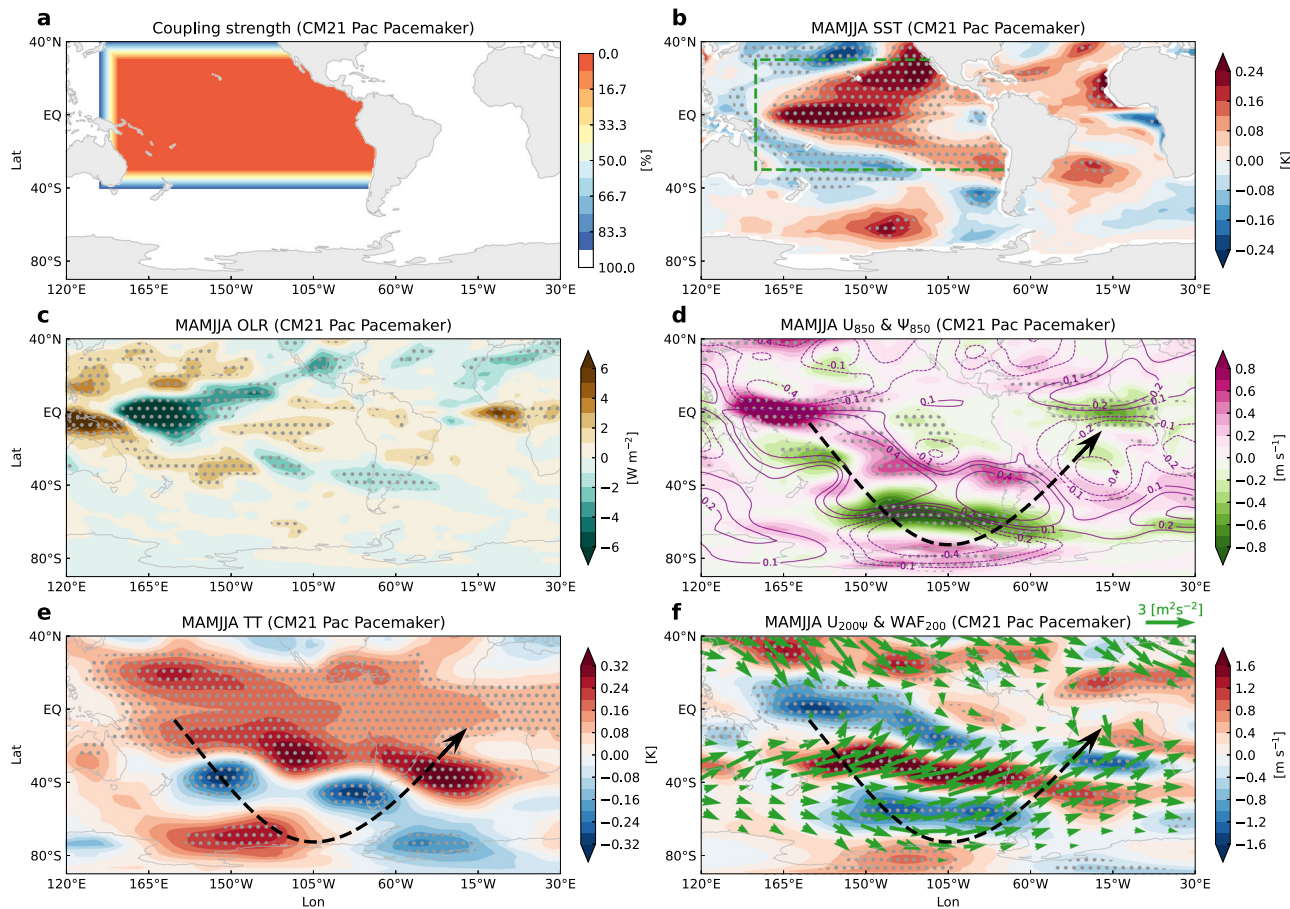


Fig. 5 | Simulated decadal inter-basin connectivity in a Pacific pacemaker experiment. **a** The applied air-sea coupling mask (shading, unit: %) in the partially CM2.1 coupled model with prescribed CP ENSO-like SST anomaly forcing; ensemble mean of anomalous **b** SST (shading, unit: K), **c** OLR (shading, unit: $W m^{-2}$), **d** 850 hPa zonal wind (shading, unit: $m s^{-1}$) and stream function (contours, unit: $10^6 m^2 s^{-1}$), **e** TT (shading, unit: K) vertically averaged between 850 hPa and

200 hPa, and **f** 200 hPa rotating zonal wind (shading, unit: $m s^{-1}$) and wave activity flux (vectors, unit: $m^2 s^{-2}$) during the MAMJJA season. The green dashed lines in **b** enclose the region of no active air-sea coupling with a mask value of zero. Black dashed arrows in **(d-f)** illustrate the southern hemisphere extratropical teleconnection pathway. Stippled shading and green vectors indicate the values exceeding the 90% confidence level based on a two-tailed Student's *t*-test.

Laboratory coupled general circulation model CM2.1⁷⁸ and its atmospheric component AM2.1⁷⁹. Both models can reasonably simulate the large-scale atmospheric circulation responses to tropical SST anomalies and have been widely used in climate research^{80–82}.

Key large-scale features of the observed inter-basin teleconnections are reasonably reproduced in both a partially coupled Pacific pacemaker experiment and atmospheric model-only simulations (see “Methods”; Fig. 5 and Supplementary Fig. 11). With an imposed CP ENSO-like decadal SST forcing (Fig. 5a, b), the resulting enhanced central-western equatorial Pacific convection (Fig. 5c) excites atmospheric tropical Kelvin and extratropical Rossby waves (Fig. 5d-f) reaching into the Atlantic, both of which dynamically favor equatorial Atlantic anomalous easterlies that cool South Atlantic SSTs by activating local Bjerknes feedback. Nevertheless, noticeable model biases are evident. In particular, the Atlantic negative SST response is generally weaker and narrower (Fig. 5b) due to its late development in boreal summer (i.e., June–August; Fig. 6a, b), despite similar atmospheric teleconnection and local wind forcing throughout the MAMJJA season (Supplementary Fig. 12). This arises from a model bias of climatological oceanic downwelling in the eastern equatorial Atlantic cold tongue region during the boreal spring (Fig. 6c, e), which hinders the initiation of TF to cool SSTs. In the subtropical region (Supplementary Fig. 13), the simulated South Atlantic Subtropical Anticyclone causes stronger oceanic warming than observed, mainly due to oceanic downwelling and the Ekman feedback process (Supplementary Fig. 13a, b, f, g). It tends to offset the atmospheric cooling effect contributed mainly by the wind-driven latent heat flux

anomalies (Supplementary Fig. 13c–e), resulting in no apparent subtropical SST cooling response. In addition, the latent heat flux on the east coast of the subtropical South Atlantic also shows a stronger than observed warming effect (Supplementary Fig. 13c, d, h, i) on the underlying SST, possibly due to a more stabilized atmosphere, as the model simulates a TT signal that penetrates the Atlantic more than observed (Figs. 4f and 5e). A similar overly strong TT effect is also found in other climate models, which dominates the simulated same-sign tropical Atlantic SST responses^{83,84} to tropical Pacific decadal SST. These results suggest that while the model can generally capture the large-scale atmospheric teleconnection pathways, it remains a challenge to realistically simulate their detailed teleconnection structures and SST feedback processes at the regional scale, thus hindering a realistic representation of the observed Pacific–Atlantic decadal connection.

In addition to a fixed CP ENSO-like SST forcing, we also analyze a tropical Pacific “time series” pacemaker experiment of the same model, incorporating the historical evolution of tropical Pacific SST anomalies (see “Methods”). Despite the overall weak cooling SST responses of the equatorial Atlantic SST due to the model biases discussed above, we still find model evidence that mimics the Pacific–South Atlantic teleconnection in the observations (Supplementary Fig. 14). In particular, the fast extratropical atmospheric teleconnection pathway in the southern hemisphere is well captured, with the underlying SST showing a concurrent connection with the Pacific signal. Instead, as in the observed case, the tropical warm TT pathway is relatively delayed, as evidenced by the delayed warming of the tropical North Atlantic SST anomalies. Importantly, even in this Pacific–

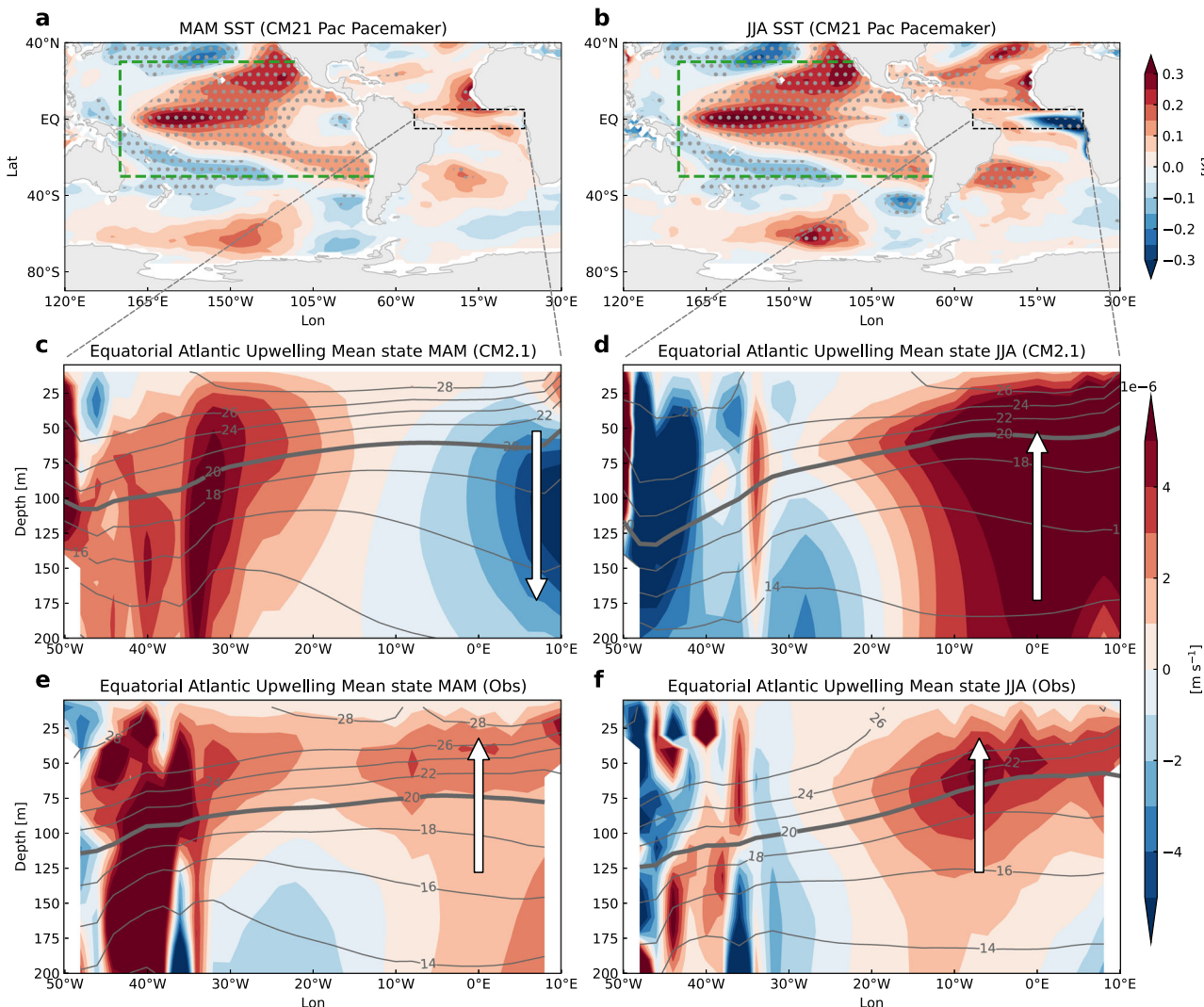


Fig. 6 | Influence of equatorial Atlantic mean upwelling bias on the simulated inter-basin decadal connection. Ensemble mean of the anomalous SST (shading, unit: K) response in the Pacific pacemaker experiment during the **a** MAM and **b** JJA seasons. The green dashed lines in **(a, b)** enclose the region of no active air-sea coupling with a mask value of zero while the black dashed box encloses the equatorial Atlantic region (50° W– 10° E, 5° S– 5° N). Stippled shading indicates values exceeding the 90% confidence level based on a two-tailed Student's *t*-test.

Meridionally averaged equatorial (5° S– 5° N) Atlantic vertical velocity (shading, unit: 10^{-6} m s $^{-1}$) and ocean temperature (contours, unit: K) climatology from the last 50 years of simulation of the Pacific-driven control experiment using the CM2.1 model during the **c** MAM and **d** JJA seasons. **e, f** as **(c, d)** but using the GECCO3 reanalysis data from 1951 to 2018. The thermocline represented by the 20° C isotherm line is thickened in **(c–f)**.

driven model world with limited Atlantic feedback, equatorial South Atlantic SST responses can lead the Pacific forcing signal by about 2 years. This may support our observational argument that the phase differences between the competing extratropical wave teleconnection and tropical TT pathways result in a subtle lead-lag relationship between tropical Pacific and South Atlantic decadal variability.

We also examine the potential role of South Atlantic SSTs in forcing the Pacific using similar partially coupled Atlantic-driven pacemaker experiments (see “Methods”; Fig. 7), which shows a rather weak response with statistically significant responses mostly confined to the Atlantic basin (Supplementary Fig. 15a–c), but no systematic SST changes in the Pacific (Fig. 7b). Consistent results were obtained using only the atmospheric model (see “Methods”, Supplementary Fig. 15d–f). The tropical South Atlantic decadal SST anomalies act mainly to modulate the climate in their vicinity and generally have limited direct feedback effects on Pacific SST, possibly due to the relatively small decadal SST magnitude of about 0.15° C (Figs. 1a and 7b) superimposed on the Atlantic cold tongue mean state. This is also consistent with a

previous study⁸⁵ arguing that a broad tropical Atlantic SST forcing is necessary in both hemispheres to ensure that its influence reaches the Pacific. Furthermore, we conducted two additional atmospheric model experiments (see “Methods”) using the Atlantic decadal SST and climatology before and after 1985 to account for the decadal changes in the Atlantic quasi-decadal SST pattern (see discussion in the next section) and the continuous warming of the tropical Atlantic background SST. Nevertheless, we still find no significant responses of the tropical CP low-level westerlies in these simulations (Supplementary Fig. 16), suggesting an overall secondary role of the direct Atlantic feedback on this quasi-decadal timescale in our model. Given the complexity of the climate system, which cannot be perfectly captured in models, and a single atmospheric model version used here, we do not completely exclude the possibility of an Atlantic feedback on the Pacific in the observations, whose role, if any, is expected to be secondary compared to the Pacific counterparts and may operate, for example, through nonlinear rectification from interannual to decadal timescales, and remains open for further investigation.

Fig. 7 | Simulated decadal inter-basin connectivity in an Atlantic pacemaker experiment. **a** The applied air–sea coupling mask (shading, unit: %) in a partially coupled CM2.1 model with prescribed tropical South Atlantic SST anomaly forcing; **b** Ensemble mean of the anomalous SST (shading, unit: K) response during the MAMJJJA season. The green dashed lines in **(b)** enclose the region of no active air–sea coupling with a mask value of zero. Stippled shading indicates values exceeding the 90% confidence level based on a two-tailed Student's *t*-test.

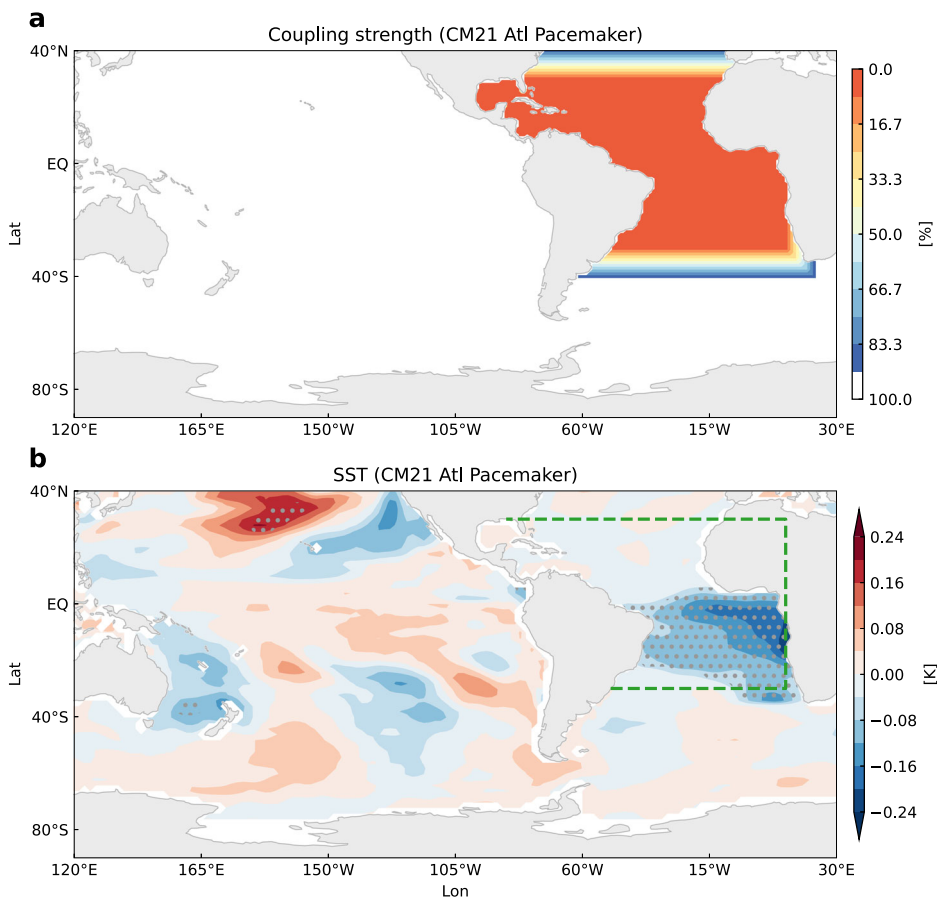
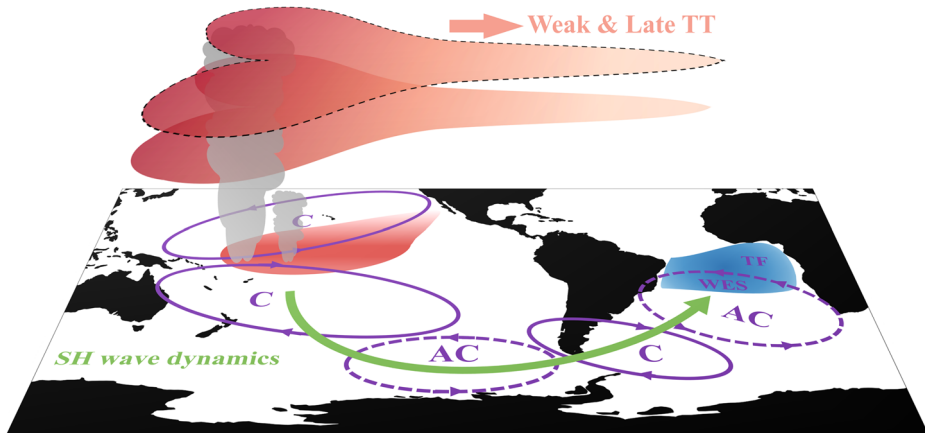


Fig. 8 | Schematic of the Pan-Pacific–Atlantic decadal connection. The CP ENSO-like decadal SST anomalies (red shading on the map) enhance local atmospheric deep convection (gray cloud-like shading) and drive low-level atmospheric circulation changes (purple ellipses), with cyclonic (solid) and anticyclonic (dashed) circulation anomalies marked with “C” and “AC”. The green arching arrow indicates the extratropical teleconnection pathway, where wave energy propagates from the Pacific to the South Atlantic. Low-level easterly anomalies on the northern flank of the subtropical South Atlantic anticyclonic circulation cool local SST anomalies (blue shading on the map) mainly through wind-evaporation SST (WES) and TF in subtropical and near-equatorial regions, respectively. The warm TT signal driven by the Pacific decadal SST anomaly manifests as a coupled Kelvin–Rossby response in the middle to upper levels (red shading above the map), which decays rapidly away from the Pacific heating center and has a weak warming effect on the tropical South Atlantic SST.



Discussion

Based on observational analysis over the past seven decades and idealized pacemaker experiments, we propose here a synchronization relationship between the tropical CP and the South Atlantic decadal variability (Fig. 8). Compared to the interannual ENSO SST, which is larger in amplitude and located in the eastern Pacific (Supplementary Fig. 9), CP ENSO-like decadal SST anomalies can effectively excite southern hemisphere extratropical

teleconnections that propagate into the South Atlantic, with a less destructive tropical TT effect due to the weaker (~ 0.5 °C) and more westward location of the SST forcing. Such a teleconnection configuration may favor a more pronounced inter-basin connection on this quasi-decadal timescale, while comparable and competing wave and TT effects on inter-annual timescales lead to a more fragile interannual relationship^{16,67}. According to our previous study²⁶, the observed CP ENSO-like decadal

variability may originate from ENSO nonlinearity amplified by tropical Pacific air-sea coupled processes, with the intermittent occurrence of strong El Niño events shaping its observed decadal timescale. This, combined with our results here, suggests a tropical CP origin of the preferred quasi-decadal timescale of tropical South Atlantic variability, different from previous arguments emphasizing physical processes within the Atlantic basin^{49–51}. Given the complexity and multiple mechanisms of the decadal variability³⁸, their relative importance deserves further investigation.

The Pan-Pacific–Atlantic teleconnection and the local Atlantic feedback processes are strongly dependent on the climatological background conditions, which exhibit a pronounced seasonality. In observations, the causes of the more pronounced inter-basin connection in the austral cold months could be twofold, including a stronger southern hemisphere mid-latitude jet stream favoring the extratropical Rossby wave teleconnection and stronger equatorial Atlantic mean upwelling favoring the oceanic TF. In most climate models, the eastern boundary upwelling systems, including those in the tropical Atlantic, have large biases that have persisted through several model generations^{86,87}, which are also manifested in the CM2.1 model during the MAM season (Fig. 6c, e). Such model biases degrade the simulated inter-basin connection by misrepresenting local TF and can arise from coarse ocean model resolution⁸⁸, missing ocean model physics, and/or biased atmospheric forcing, the latter further complicated by the complex orography and landscapes surrounding the Atlantic basin, including the Sahara desert and the Amazon rainforest, which have impacts on climate in the tropical South Atlantic. Thus, there is a compelling need to better understand and resolve these model biases to ensure a realistic simulation of inter-basin linkages and more reliable predictions of the surrounding climate.

On interannual timescales, the Pacific–Atlantic connection is non-stationary and exhibits decadal variations^{89–91} due to decadal changes in the Atlantic background conditions and the modulated structural changes in equatorial Atlantic SST anomalies. In a similar context, we also examine our results by dividing the entire study period (i.e., 1951–2022) into two comparable decadal epochs, namely 1951–1985 and 1986–2022 (Supplementary Fig. 17). Interestingly, the tropical Atlantic decadal SST shows a meridional dipole structure in the first epoch, but manifests as a monopole structure in the second epoch, with a strong emphasis in the tropical South Atlantic and weaker signals in the tropical North Atlantic. This is consistent with our previously presented results that the quasi-decadal variability of the tropical CP and the tropical South Atlantic show relatively robust coevolution throughout the period (Fig. 2c), while the tropical North Atlantic is not connected to the tropical CP from the MCA analysis (Supplementary Figs. 1 and 3). The decadal Pacific–Atlantic evolutions in the first epoch are also consistent with previous studies showing pronounced quasi-decadal variations in the Atlantic meridional mode in early observational reanalysis data. Moreover, the significant signals appear to be established earlier in the tropical South Atlantic than in the tropical North Atlantic (Supplementary Fig. 17a), suggesting an earlier arrival of extratropical teleconnection pathway from the southern hemisphere. So far, the physical reasons for the non-stationary decadal coupling between the tropical CP and the tropical North Atlantic are not clear, but may be related to decadal teleconnection changes in the tropical warm Kelvin wave, extratropical wave propagation paths in the northern hemisphere, and/or tropical Atlantic background conditions (e.g., mean SST or precipitation) that control the thermodynamic air-sea coupling strength between the two hemispheres. Given that each decadal epoch contains very few effective samples of about 3 decadal cycles, statistical significance tests cannot be fully relied upon to determine whether these changes are due to confounding noisy processes or related to systematic changes in background conditions, and this issue merits careful study in the future.

Methods

Reanalysis data

In this study, atmospheric reanalysis data from 1951 to 2022 is from the fifth generation of the European Centre for Medium-Range Weather Forecasts

(ECMWF) reanalysis (ERA5)⁹². Monthly SSTs for the same period were used from the National Oceanic and Atmospheric Administration (NOAA) Extended Reconstructed SST dataset, version 5 (ERSSTv5)⁹³ and the Hadley Center Sea Ice and Sea Surface Temperature dataset (HadISST)⁹⁴. In addition, the ocean reanalysis from the German contribution to the Estimating the Circulation and Climate of the Ocean project, version 3 (GECCO3)⁹⁵, which covers the 1951–2018 period due to data availability, was used to quantify the oceanic feedback contribution to decadal tropical South Atlantic SST changes. All variables were linearly interpolated onto a common grid with a horizontal spatial resolution of $2^\circ \times 2^\circ$ and a vertical resolution of 10 m in the upper ocean (down to 350 m depth). Anomalies were calculated relative to the full period climatology and linearly detrended. To extract variability on the quasi-decadal timescale (Figs. 1 and 2), we used an 8–16-year Lanczos bandpass filter⁹⁶. Our results do not change much when we use other filter cutoff periodicities, such as 8–20 years²⁶ or 10–15 years⁴⁵.

Decadal heat budget analysis

On decadal timescales, the ocean-atmosphere circulations are in a quasi-equilibrium state⁹⁷. In particular, the Newtonian cooling effect on decadal SST anomalies is generally balanced by ocean dynamics and atmospheric heat flux driven by large-scale ocean-atmosphere circulation anomalies. Thus, decadal mixed-layer ocean temperature anomalies or their equivalent SST anomalies can be decomposed into different oceanic and atmospheric feedback processes using a decadal mixed-layer heat budget analysis:

$$T'_{mld} = \frac{D_o + Q_{sw} + Q_{lw} + Q_{sh} + Q_{lh}^a}{-\alpha \bar{Q}_{lh}} \quad (1)$$

The D_o , Q_{sw} , Q_{lw} , Q_{sh} and Q_{lh}^a terms in Eq. 1 represent the collective role of the large-scale ocean dynamics, the net shortwave flux, the net longwave flux, the sensible heat flux, and the atmospheric forcing of the latent heat flux anomalies at the sea surface down into the ocean, respectively. The \bar{Q}_{lh} term is the climatological net sea surface latent heat flux and α has an approximately constant value of 0.06 K^{-1} in tropical oceans⁹⁷.

The oceanic feedback (D_o) is calculated in partial flux form (Eq. 2)⁹⁸, which includes the dynamical damping effect of the mean ocean circulation, the TF, the advective feedback in three directions, and nonlinear dynamical heating terms:

$$D_o = - \left(\frac{\partial(uT')}{\partial x} + \frac{\partial(vT')}{\partial y} \right) + \frac{\bar{w}T'_{lh}}{H} - \left(u' \frac{\partial \bar{T}}{\partial x} + v' \frac{\partial \bar{T}}{\partial y} + w' \frac{\partial \bar{T}}{\partial z} \right) - \left(u' \frac{\partial T'}{\partial x} + v' \frac{\partial T'}{\partial y} + w' \frac{\partial T'}{\partial z} \right) \quad (2)$$

As in our previous study²⁶, the variables T , u , and v denote the anomalous ocean temperature, and zonal, and meridional ocean current velocities averaged in the mixed layer, respectively. T_{lh} and w represent the ocean temperature and vertical current anomalies at the bottom of the mixed layer. Variables with an overbar and a prime indicate climatology and anomalies, respectively. Following previous studies^{99–101}, the mixed layer depth H is set to a constant value of 50 m, which is close to the average value for the tropical South Atlantic. This setting does not affect our results much from a basin-scale integrated perspective, but may be less accurate in the very coastal regions of the eastern Atlantic (e.g., the Benguela Niño region), where the assessment of the oceanic feedback is also limited by the coarse resolution of the ocean reanalysis data and the numerical difference scheme around the coastal regions.

The latent heat flux includes both the SST response (Q_{lh}^o) and the atmospheric forcing (Q_{lh}^a), and the latter can be calculated by subtracting the SST response (i.e., Newtonian cooling) from the total latent heat flux. The atmospheric forcing is further decomposed into the wind effect (Q_{lh}^W) and a residual (*resid*) that includes the effects of relative humidity, surface static stability, and other factors. In Eq. 3, the T'_s , \bar{W} , and W' represent SST anomalies, climatological surface wind speed, and surface wind speed anomalies, respectively, while other symbols have the same meaning as in

Eq. 1:

$$Q_{lh}^a = \begin{cases} Q_{lh} - Q_{lh}^o = Q_{lh} - \alpha \overline{Q_{lh}} T'_s \\ Q_{lh}^W + resid = \overline{Q_{lh}} W' + resid \end{cases} \quad (3)$$

Wave activity flux

To determine the source and direction of wave energy propagation, the wave activity flux was calculated using the Takaya and Nakamura (TN-WAF)¹⁰² method. It is a useful tool to diagnose the propagation direction of the Rossby wave packet in a non-uniform zonal air flow and infer where the wave energy is emitted and absorbed. Its horizontal components are defined as:

$$F = \frac{p \cos \varphi}{2|U|} \begin{cases} \frac{U}{a^2 \cos \varphi^2} \left[\left(\frac{\partial \psi'}{\partial \lambda} \right)^2 - \psi' \frac{\partial^2 \psi'}{\partial \lambda^2} \right] + \frac{V}{a^2 \cos \varphi} \left(\frac{\partial \psi'}{\partial \lambda} \frac{\partial \psi'}{\partial \varphi} - \psi' \frac{\partial^2 \psi'}{\partial \lambda \partial \varphi} \right) \\ \frac{U}{a^2 \cos \varphi} \left(\frac{\partial \psi'}{\partial \lambda} \frac{\partial \psi'}{\partial \varphi} - \psi' \frac{\partial^2 \psi'}{\partial \lambda \partial \varphi} \right) + \frac{V}{a^2} \left[\left(\frac{\partial \psi'}{\partial \varphi} \right)^2 - \psi' \frac{\partial^2 \psi'}{\partial \varphi^2} \right] \end{cases} \quad (4)$$

where $p = 0.2$ is the upper-level pressure (200 hPa) normalized by 1000 hPa, a is the radius of the Earth (6371200 m), φ and λ are the latitude and the longitude coordinates in radians. $|U|$, U , and V represent basic states of the upper-level total, zonal, and meridional wind speed, while ψ' denotes the geostrophic stream function anomaly.

Statistical significance tests

The composite and correlation analyses in our study are all tested using the two-tailed Student's t -test. Before determining the statistical significance of correlations on our target decadal timescale, the adjusted effective degrees of freedom¹⁰³ were calculated as:

$$\frac{1}{N^{edf}} \approx \frac{1}{N} + \frac{2}{N} \sum_{j=1}^N \frac{(N-j)}{N} \rho_{XX}(j) \rho_{YY}(j) \quad (5)$$

where N and N^{edf} are the sample size (i.e., 72 years) and effective degrees of freedom, and the $\rho_{XX}(j)$ and $\rho_{YY}(j)$ are the autocorrelations of 8–16-year bandpass filtered samples X and Y at lag time step j , respectively.

In our study, the SST index spectra and their relationships all exceed the 95% confidence level after accounting for the effective degrees of freedom, suggesting the robustness of the identified quasi-decadal variability and inter-basin linkages. Considering the weaker signal-to-noise ratio on decadal timescales compared to interannual timescales and limited effective sample size in observations, we relax our statistical confidence level to 90% in the analysis of decadal Pan-Pacific–Atlantic phase evolutions and associated large-scale ocean-atmospheric circulations. The effective degrees of freedom are evaluated at each grid point, except for the MCA heterogeneous correlation patterns (Fig. 2a, b), where a roughly estimated fixed effective sample size of 6 (72 years divided by 12 years/cycle) is assumed to smoothly enclose the core regions of inter-basin decadal connectivity for better visual effects.

Model experimental designs

The CM2.1 model is used for the partially coupled Pacific-driven and Atlantic-driven pacemaker experiments, for which air-sea coupling strength is controlled by air-sea coupling masks (Figs. 5a and 7a). A mask value of 100% means that the ocean and atmosphere are fully coupled, while a coupling strength of 0% means that the model's SST boundary conditions are simply prescribed to force the atmosphere unidirectionally, as in an AGCM experiment. The intermediate buffer zone is set to avoid large unphysical spatial gradients in SST boundary forcing and denotes the partitioning fraction of model-generated and prescribed SSTs.

In the Pacific-driven control simulation, the tropical Pacific SST is restored to the observed seasonal climatology from 1951 to 2022, while elsewhere the ocean and atmosphere are freely coupled. The use of the observational rather than the model SST climatology here is to reduce the influence of possible model biases in the background SST states of the forcing region^{85,86,104}. The control run was integrated for 100 years, with the first 50 years of simulations used for spin-up and not used in the analysis. The Pacific-driven perturbation experiment is set up by adding the decadal CP ENSO-like SST forcing to the observed SST climatology with the same tropical Pacific air-sea coupling mask. This perturbation run has 50 ensemble members with different initial conditions, branched from the last 50 years of the control run. Each member is integrated for 6 months from March to August. The Atlantic-driven pacemaker simulation has almost the same model configuration as the Pacific-driven experiment, except for the air-sea coupling mask and the decadal SST anomaly forcing. To ensure a realistic magnitude of decadal SST forcing patterns, the Pacific and Atlantic decadal SST forcings (Figs. 5b and 7b) are derived by regressing the 8–16-year filtered MAMJJA SST onto the simultaneous normalized Niño4 (160° E–150° W, 5° S–5° N) and tropical South Atlantic (40° W–10° E, 15° S–0° N) SST indices, respectively.

To understand the observed subtle one-year phase difference between the two basins, we additionally analyzed the 10-member tropical Pacific “time series” pacemaker experiment of the same CM2.1 model from previous studies^{80,82}. Different from our experiments with a fixed CP ENSO-like SST forcing, their “time series” Pacific pacemaker experiment includes the observed evolution of SST anomalies in the tropical central-eastern Pacific for the historical period from 1951 to 2014. Although this experiment has a slightly different air-sea coupling mask domain and data source of SST anomaly forcing compared to our experiment, it generally captures the observed tropical Pacific decadal variability and allows us to test our hypothesis that the statistical one-year lead of the equatorial Atlantic decadal variability can arise solely from Pacific forcing in the presence of delayed and competing effect between the tropical and subtropical pathways. More details on this Pacific “time series” pacemaker experiment can be found in relevant literature.

In the partially coupled experiments, the SST responses outside the restoration region also contribute to the atmospheric teleconnection responses. To isolate the sole effects of Pacific and Atlantic SST, we also conducted three experiments using only the atmospheric model component to facilitate comparisons with our coupled simulations. The experiments are a control simulation and two SST perturbation experiments. In the control simulation, the model was driven by a repeated global seasonal SST climatology computed over the study period (i.e., 1951–2022) and was integrated for 65 years. The first 5 years of the simulations were discarded as a spin-up period. In the two SST perturbation experiments, SST boundary conditions were created by adding the decadal SST anomaly patterns (Figs. 5b and 7b) to the observed SST climatology in the tropical Pacific (150° E–80° W, 30° S–30° N) and Atlantic (65° W–30° E, 30° S–10° N), respectively. Each simulation has 60 ensemble members with different initial conditions, branched from the control simulation. Each member is integrated for 12 months from January to December. In addition, to account for the decadal changes in the tropical Atlantic decadal SST pattern and the continuous warming of the background SST states, we conducted two more pairs of control and Atlantic SST perturbation experiments, similar to the configuration above, except that the SST climatology and Atlantic decadal SST patterns used (Supplementary Fig. 16a, e) were from before and after 1985.

Data availability

Reanalysis data sets used in this article are all publicly available: the ERSSTv5 at <https://psl.noaa.gov/data/gridded/data.noaa.ersst.v5.html>; the Hadley Centre SST at https://www.metoffice.gov.uk/hadobs/hadisst/data/HadISST_sst.nc.gz; the GECCO3 at <https://www.cen.uni-hamburg.de/en/icdc/data/ocean/reanalysis-ocean/gecco3.html>; the ERA5 at <https://cds.climate.copernicus.eu/#/search?text=ERA5&type=dataset>. The ten-

member “time series” Pacific pacemaker experiment output is available at <https://zenodo.org/records/6004084>. Data for the CP-ENSO and tropical South Atlantic-driven pacemaker experiments are available at <https://figshare.com/s/3bf4a6b7367b7de6e8ef>.

Code availability

The MCA/SVD analysis is implemented by the Python package “xeofs”, which is publicly available at <https://xeofs.readthedocs.io/en/latest/>. The analysis code used in this study is available from the corresponding authors upon reasonable request.

Received: 16 July 2024; Accepted: 11 October 2024;

Published online: 21 October 2024

References

1. Cai, W. et al. Pantropical climate interactions. *Science* **363**, eaav4236 (2019).
2. Wang, C. Three-ocean interactions and climate variability: a review and perspective. *Clim. Dyn.* **53**, 5119–5136 (2019).
3. Zhao, S. et al. Explainable El Niño predictability from climate mode interactions. *Nature* **630**, 891–898 (2024).
4. Zhang, W., Jiang, F., Stuecker, M. F., Jin, F.-F. & Timmermann, A. Spurious north tropical Atlantic precursors to El Niño. *Nat. Commun.* **12**, 3096 (2021).
5. García-Serrano, J., Cassou, C., Douville, H., Giannini, A. & Doblas-Reyes, F. J. Revisiting the ENSO teleconnection to the tropical North Atlantic. *J. Clim.* **30**, 6945–6957 (2017).
6. Richter, I., Tokinaga, H., Kosaka, Y., Doi, T. & Kataoka, T. Revisiting the tropical Atlantic influence on El Niño–Southern oscillation. *J. Clim.* **34**, 8533–8548 (2021).
7. Meehl, G. A. et al. Initialized earth system prediction from subseasonal to decadal timescales. *Nat. Rev. Earth Environ.* **2**, 340–357 (2021).
8. McPhaden, M. J., Zebiak, S. E. & Glantz, M. H. ENSO as an integrating concept in earth science. *Science* **314**, 1740–1745 (2006).
9. Ruiz-Barradas, A., Carton, J. A. & Nigam, S. Structure of interannual-to-decadal climate variability in the tropical atlantic sector. *J. Clim.* **13**, 3285–3297 (2000).
10. Enfield, D. B. & Mayer, D. A. Tropical Atlantic sea surface temperature variability and its relation to El Niño–Southern oscillation. *J. Geophys. Res. Oceans* **102**, 929–945 (1997).
11. Lee, S., Enfield, D. B. & Wang, C. Why do some El Niños have no impact on tropical North Atlantic SST? *Geophys. Res. Lett.* **35**, L167052 (2008).
12. Wallace, J. M. & Gutzler, D. S. Teleconnections in the geopotential height field during the northern hemisphere winter. *Mon. Weather Rev.* **109**, 784–812 (1981).
13. Klein, S. A., Soden, B. J. & Lau, N.-C. Remote sea surface temperature variations during ENSO: evidence for a tropical atmospheric bridge. *J. Clim.* **12**, 917–932 (1999).
14. Zebiak, S. E. Air-sea interaction in the equatorial Atlantic region. *J. Clim.* **6**, 1567–1586 (1993).
15. Park, J.-H. et al. Distinct decadal modulation of Atlantic-Niño influence on ENSO. *NPJ Clim. Atmos. Sci.* **6**, 105 (2023).
16. Chang, P., Fang, Y., Saravanan, R., Ji, L. & Seidel, H. The cause of the fragile relationship between the Pacific El Niño and the Atlantic Niño. *Nature* **443**, 324–328 (2006).
17. Lübbecke, J. F. & McPhaden, M. J. On the inconsistent relationship between Pacific and Atlantic Niños*. *J. Clim.* **25**, 4294–4303 (2012).
18. Tokinaga, H., Richter, I. & Kosaka, Y. ENSO influence on the Atlantic Niño, revisited: multi-year versus single-year ENSO events. *J. Clim.* **32**, 4585–4600 (2019).
19. Ham, Y.-G., Kug, J.-S., Park, J.-Y. & Jin, F.-F. Sea surface temperature in the north tropical Atlantic as a trigger for El Niño/Southern oscillation events. *Nat. Geosci.* **6**, 112–116 (2013).
20. Jiang, L., Li, T. & Ham, Y. Critical role of tropical North Atlantic SSTa in boreal summer in affecting subsequent ENSO evolution. *Geophys. Res. Lett.* **49**, e2021GL097606 (2022).
21. Rodríguez-Fonseca, B. et al. Are Atlantic Niños enhancing Pacific ENSO events in recent decades? *Geophys. Res. Lett.* **36**, L20705 (2009).
22. Ding, H., Keenlyside, N. S. & Latif, M. Impact of the equatorial Atlantic on the El Niño southern oscillation. *Clim. Dyn.* **38**, 1965–1972 (2012).
23. Wang, L., Yu, J.-Y. & Paek, H. Enhanced biennial variability in the Pacific due to Atlantic capacitor effect. *Nat. Commun.* **8**, 14887 (2017).
24. Jiang, F. et al. Resolving the tropical Pacific/Atlantic interaction conundrum. *Geophys. Res. Lett.* **50**, e2023GL103777 (2023).
25. Lyu, K., Zhang, X., Church, J. A., Hu, J. & Yu, J.-Y. Distinguishing the quasi-decadal and multidecadal sea level and climate variations in the Pacific: implications for the ENSO-like low-frequency variability. *J. Clim.* **30**, 5097–5117 (2017).
26. Liu, C., Zhang, W., Jin, F., Stuecker, M. F. & Geng, L. Equatorial origin of the observed tropical Pacific quasi-decadal variability from ENSO nonlinearity. *Geophys. Res. Lett.* **49**, e2022GL097903 (2022).
27. Mantua, N. J., Hare, S. R., Zhang, Y., Wallace, J. M. & Francis, R. C. A Pacific interdecadal climate oscillation with impacts on salmon production. *Bull. Am. Meteorol. Soc.* **78**, 1069–1079 (1997).
28. Mantua, N. J. & Hare, S. R. The Pacific decadal oscillation. *J. Oceanogr.* **58**, 35–44 (2002).
29. Power, S., Casey, T., Folland, C., Colman, A. & Mehta, V. Inter-decadal modulation of the impact of ENSO on Australia. *Clim. Dyn.* **15**, 319–324 (1999).
30. Newman, M. et al. The Pacific decadal oscillation, revisited. *J. Clim.* **29**, 4399–4427 (2016).
31. Chang, P. et al. Pacific meridional mode and El Niño–Southern oscillation. *Geophys. Res. Lett.* **34**, L16608 (2007).
32. Di Lorenzo, E. et al. Modes and mechanisms of Pacific decadal-scale variability. *Ann. Rev. Mar. Sci.* **15**, 249–275 (2023).
33. Stuecker, M. F. Revisiting the Pacific meridional mode. *Sci. Rep.* **8**, 3216 (2018).
34. Furtado, J. C., Di Lorenzo, E., Anderson, B. T. & Schneider, N. Linkages between the North Pacific oscillation and central tropical Pacific SSTs at low frequencies. *Clim. Dyn.* **39**, 2833–2846 (2012).
35. Di Lorenzo, E. et al. Central Pacific El Niño and decadal climate change in the North Pacific ocean. *Nat. Geosci.* **3**, 762–765 (2010).
36. Capotondi, A., Newman, M., Xu, T. & Di Lorenzo, E. An optimal precursor of northeast Pacific marine heatwaves and central Pacific El Niño events. *Geophys. Res. Lett.* **49**, e2021GL097350 (2022).
37. Power, S. et al. Decadal climate variability in the tropical Pacific: characteristics, causes, predictability, and prospects. *Science* **374**, eaay9165 (2021).
38. Capotondi, A. et al. Mechanisms of tropical Pacific decadal variability. *Nat. Rev. Earth Environ.* **4**, 754–769 (2023).
39. White, W. B., Tourre, Y. M., Barlow, M. & Dettinger, M. A delayed action oscillator shared by biennial, interannual, and decadal signals in the Pacific basin. *J. Geophys. Res. Oceans*. <https://doi.org/10.1029/2002JC001490> (2003).
40. Kleeman, R., McCreary, J. P. & Klinger, B. A. A mechanism for generating ENSO decadal variability. *Geophys. Res. Lett.* **26**, 1743–1746 (1999).
41. Capotondi, A., Alexander, M. A., Deser, C. & McPhaden, M. J. Anatomy and decadal evolution of the Pacific subtropical–tropical cells (STCs)*. *J. Clim.* **18**, 3739–3758 (2005).
42. Rodgers, K. B., Friederichs, P. & Latif, M. Tropical Pacific decadal variability and its relation to decadal modulations of ENSO. *J. Clim.* **17**, 3761–3774 (2004).
43. Kao, P., Hung, C. & Hong, C. Increasing influence of central Pacific El Niño on the inter-decadal variation of spring rainfall in northern Taiwan and southern China since 1980. *Atmos. Sci. Lett.* **19**, e864 (2018).

44. Liu, C., Zhang, W., Stuecker, M. F. & Jin, F. Pacific meridional mode–western north Pacific tropical cyclone linkage explained by tropical Pacific quasi-decadal variability. *Geophys. Res. Lett.* **46**, 13346–13354 (2019).

45. Wang, S.-Y., Gillies, R. R., Jin, J. & Hipps, L. E. Coherence between the Great Salt Lake level and the Pacific quasi-decadal oscillation. *J. Clim.* **23**, 2161–2177 (2010).

46. Liu, Y. et al. Decadal oscillation provides skillful multiyear predictions of Antarctic sea ice. *Nat. Commun.* **14**, 8286 (2023).

47. Lamb, P. J. West African water vapor variations between recent contrasting Subsaharan rainy seasons. *Tellus A Dyn. Meteorol. Oceanogr.* **35**, 198 (1983).

48. Folland, C. K., Palmer, T. N. & Parker, D. E. Sahel rainfall and worldwide sea temperatures, 1901–85. *Nature* **320**, 602–607 (1986).

49. Chang, P., Ji, L. & Li, H. A decadal climate variation in the tropical Atlantic Ocean from thermodynamic air–sea interactions. *Nature* **385**, 516–518 (1997).

50. Xie, S.-P. A dynamic ocean–atmosphere model of the tropical Atlantic decadal variability. *J. Clim.* **12**, 64–70 (1999).

51. Xie, S. & Tanimoto, Y. A pan-Atlantic decadal climate oscillation. *Geophys. Res. Lett.* **25**, 2185–2188 (1998).

52. Nnamchi, H. C. et al. Pan-Atlantic decadal climate oscillation linked to ocean circulation. *Commun. Earth Environ.* **4**, 121 (2023).

53. Árthun, M., Wills, R. C. J., Johnson, H. L., Chafik, L. & Langehaug, H. R. Mechanisms of decadal North Atlantic climate variability and implications for the recent cold anomaly. *J. Clim.* **34**, 3421–3439 (2021).

54. Venegas, S. A., Mysak, L. A. & Straub, D. N. Evidence for interannual and interdecadal climate variability in the South Atlantic. *Geophys. Res. Lett.* **23**, 2673–2676 (1996).

55. Venegas, S. A., Mysak, L. A. & Straub, D. N. Atmosphere–ocean coupled variability in the South Atlantic. *J. Clim.* **10**, 2904–2920 (1997).

56. Sterl, A. & Hazeleger, W. Coupled variability and air–sea interaction in the South Atlantic Ocean. *Clim. Dyn.* **21**, 559–571 (2003).

57. Haarsma, R. J. et al. Dominant modes of variability in the South Atlantic: a study with a hierarchy of ocean–atmosphere models. *J. Clim.* **18**, 1719–1735 (2005).

58. Nnamchi, H. C., Li, J. & Anyadike, R. N. C. Does a dipole mode really exist in the South Atlantic ocean? *J. Geophys. Res.* **116**, D15104 (2011).

59. Nnamchi, H. C., Kucharski, F., Keenlyside, N. S. & Farneti, R. Analogous seasonal evolution of the South Atlantic SST dipole indices. *Atmos. Sci. Lett.* **18**, 396–402 (2017).

60. Reboita, M. S., Ambrizzi, T., Silva, B. A., Pinheiro, R. F. & da Rocha, R. P. The South Atlantic subtropical anticyclone: present and future climate. *Front. Earth Sci.* <https://doi.org/10.3389/feart.2019.00008> (2019).

61. Nnamchi, H. C. et al. An equatorial–extratropical dipole structure of the Atlantic Niño. *J. Clim.* **29**, 7295–7311 (2016).

62. Shannon, L. V., Boyd, A. J., Brundrit, G. B. & Taunton-Clark, J. On the existence of an El Niño-type phenomenon in the Benguela System. *J. Mar. Res.* **44**, 495–520 (1986).

63. Venegas, S. A., Mysak, L. A. & Straub, D. N. An interdecadal climate cycle in the South Atlantic and its links to other ocean basins. *J. Geophys. Res. Oceans* **103**, 24723–24736 (1998).

64. Rouault, M. & Tomyet, F. S. Impact of El Niño–Southern oscillation on the Benguela upwelling. *J. Phys. Oceanogr.* **52**, 2573–2587 (2022).

65. Richter, I. et al. On the triggering of Benguela Niños: remote equatorial versus local influences. *Geophys. Res. Lett.* **37**, L20604 (2010).

66. Rodrigues, R. R., Campos, E. J. D. & Haarsma, R. The impact of ENSO on the South Atlantic subtropical dipole mode. *J. Clim.* **28**, 2691–2705 (2015).

67. Jiang, L., Li, T. & Ham, Y.-G. Asymmetric impacts of El Niño and La Niña on equatorial Atlantic warming. *J. Clim.* **36**, 193–212 (2023).

68. Zhao, Y. & Capotondi, A. The role of the tropical Atlantic in tropical Pacific climate variability. *NPJ Clim. Atmos. Sci.* **7**, 140 (2024).

69. Chiang, J. C. H. & Vimont, D. J. Analogous Pacific and Atlantic Meridional modes of tropical atmosphere–ocean variability*. *J. Clim.* **17**, 4143–4158 (2004).

70. Cai, W. et al. Climate impacts of the El Niño–Southern oscillation on South America. *Nat. Rev. Earth Environ.* **1**, 215–231 (2020).

71. Mann, M. E. & Park, J. Oscillatory spatiotemporal signal detection in climate studies: a multiple-taper spectral domain approach. *Adv. Geophys.* [https://doi.org/10.1016/S0065-2687\(08\)60026-6](https://doi.org/10.1016/S0065-2687(08)60026-6) (1999).

72. Mann, M. E., Steinman, B. A. & Miller, S. K. Absence of internal multidecadal and interdecadal oscillations in climate model simulations. *Nat. Commun.* **11**, 49 (2020).

73. Mann, M. E., Steinman, B. A., Brouillette, D. J. & Miller, S. K. Multidecadal climate oscillations during the past millennium driven by volcanic forcing. *Science* **371**, 1014–1019 (2021).

74. Ding, Q., Steig, E. J., Battisti, D. S. & Küttel, M. Winter warming in West Antarctica caused by central tropical Pacific warming. *Nat. Geosci.* **4**, 398–403 (2011).

75. Clem, K. R., Bozkurt, D., Kennett, D., King, J. C. & Turner, J. Central tropical Pacific convection drives extreme high temperatures and surface melt on the Larsen C ice shelf, Antarctic Peninsula. *Nat. Commun.* **13**, 3906 (2022).

76. Gill, A. E. Some simple solutions for heat-induced tropical circulation. *Q. J. R. Meteorol. Soc.* **106**, 447–462 (1980).

77. Chiang, J. C. H. & Sobel, A. H. Tropical tropospheric temperature variations caused by ENSO and their influence on the remote tropical climate. *J. Clim.* **15**, 2616–2631 (2002).

78. Delworth, T. L. et al. GFDL’s CM2 global coupled climate models. Part I: formulation and simulation characteristics. *J. Clim.* **19**, 643–674 (2006).

79. GAMDT. The new GFDL global atmosphere and land model AM2–LM2: eEvaluation with prescribed SST simulations. *J. Clim.* **17**, 4641–4673 (2004).

80. Kosaka, Y. & Xie, S.-P. Recent global-warming hiatus tied to equatorial Pacific surface cooling. *Nature* **501**, 403–407 (2013).

81. Stuecker, M. F. et al. Revisiting ENSO/Indian Ocean dipole phase relationships. *Geophys. Res. Lett.* **44**, 2481–2492 (2017).

82. Zhang, Y. et al. Atmospheric forcing of the Pacific meridional mode: tropical Pacific-driven versus internal variability. *Geophys. Res. Lett.* **49**, e2022GL098148 (2022).

83. Meehl, G. A. et al. Atlantic and Pacific tropics connected by mutually interactive decadal-timescale processes. *Nat. Geosci.* **14**, 36–42 (2021).

84. Yao, S.-L., Chu, P.-S., Wu, R. & Zheng, F. Model consistency for the underlying mechanisms for the inter-decadal Pacific Oscillation–tropical Atlantic connection. *Environ. Res. Lett.* **17**, 124006 (2022).

85. Jiang, L. & Li, T. Impacts of tropical North Atlantic and equatorial Atlantic SST anomalies on ENSO. *J. Clim.* **34**, 5635–5655 (2021).

86. McGregor, S., Stuecker, M. F., Kajtar, J. B., England, M. H. & Collins, M. Model tropical Atlantic biases underpin diminished Pacific decadal variability. *Nat. Clim. Chang* **8**, 493–498 (2018).

87. Farneti, R., Stiz, A. & Ssebandeke, J. B. Improvements and persistent biases in the southeast tropical Atlantic in CMIP models. *NPJ Clim. Atmos. Sci.* **5**, 42 (2022).

88. Jing, Z. et al. Geostrophic flows control future changes of oceanic eastern boundary upwelling. *Nat. Clim. Chang* **13**, 148–154 (2023).

89. Martín-Rey, M., Rodríguez-Fonseca, B. & Polo, I. Atlantic opportunities for ENSO prediction. *Geophys. Res. Lett.* **42**, 6802–6810 (2015).

90. Polo, I., Martín-Rey, M., Rodríguez-Fonseca, B., Kucharski, F. & Mechoso, C. R. Processes in the Pacific La Niña onset triggered by the Atlantic Niño. *Clim. Dyn.* **44**, 115–131 (2015).

91. Martín-Rey, M., Rodríguez-Fonseca, B., Polo, I. & Kucharski, F. On the Atlantic–Pacific Niños connection: a multidecadal modulated mode. *Clim. Dyn.* **43**, 3163–3178 (2014).

92. Hersbach, H. et al. The ERA5 global reanalysis. *Q. J. R. Meteorol. Soc.* **146**, 1999–2049 (2020).

93. Huang, B. et al. Extended reconstructed sea surface temperature, version 5 (ERSSTv5): upgrades, validations, and intercomparisons. *J. Clim.* **30**, 8179–8205 (2017).

94. Rayner, N. A. et al. Global analyses of sea surface temperature, sea ice, and night marine air temperature since the late nineteenth century. *J. Geophys. Res. Atmos.* <https://doi.org/10.1029/2002JD002670> (2003).

95. Köhl, A. Evaluating the GECCO3 1948–2018 ocean synthesis—a configuration for initializing the MPI-ESM climate model. *Q. J. R. Meteorol. Soc.* **146**, 2250–2273 (2020).

96. Duchon, C. E. Lanczos filtering in one and two dimensions. *J. Appl. Meteorol.* **18**, 1016–1022 (1979).

97. Xie, S.-P. et al. Global warming pattern formation: sea surface temperature and rainfall*. *J. Clim.* **23**, 966–986 (2010).

98. An, S.-I., Jin, F.-F. & Kang, I.-S. The role of zonal advection feedback in phase transition and growth of ENSO in the Cane–Zebiak model. *J. Meteorol. Soc. Jpn. Ser. II* **77**, 1151–1160 (1999).

99. Nnamchi, H. C. et al. Thermodynamic controls of the Atlantic Niño. *Nat. Commun.* **6**, 8895 (2015).

100. Zhang, L. & Han, W. Indian Ocean dipole leads to Atlantic Niño. *Nat. Commun.* **12**, 5952 (2021).

101. Zhang, L. et al. Emergence of the Central Atlantic Niño. *Sci. Adv.* **9**, eadi5507 (2023).

102. Takaya, K. & Nakamura, H. A formulation of a phase-independent wave-activity flux for stationary and migratory quasigeostrophic eddies on a zonally varying basic flow. *J. Atmos. Sci.* **58**, 608–627 (2001).

103. Pyper, B. J. & Peterman, R. M. Comparison of methods to account for autocorrelation in correlation analyses of fish data. *Can. J. Fish. Aquat. Sci.* **55**, 2127–2140 (1998).

104. Kajtar, J. B., Santoso, A., McGregor, S., England, M. H. & Baillie, Z. Model under-representation of decadal Pacific trade wind trends and its link to tropical Atlantic bias. *Clim. Dyn.* **50**, 1471–1484 (2018).

Korean government (MSIT) (NRF-2023R1A2C1004083). Leishan Jiang was supported by NSFC42305021 and SBK2023043823.

Author contributions

C.L. conceived the idea, designed the study, conducted the analysis and model simulations, and prepared all the figures. C.L., S.-K.K., and M.F.S. drafted the manuscript. S.-I.A. directed the research and supervised the project. All authors contributed to the interpretation of results and to the manuscript improvement.

Competing interests

The authors declare no competing interests.

Additional information

Supplementary information The online version contains supplementary material available at <https://doi.org/10.1038/s41612-024-00806-y>.

Correspondence and requests for materials should be addressed to Chao Liu or Soon-Il An.

Reprints and permissions information is available at <http://www.nature.com/reprints>

Publisher's note Springer Nature remains neutral with regard to jurisdictional claims in published maps and institutional affiliations.

Open Access This article is licensed under a Creative Commons Attribution-NonCommercial-NoDerivatives 4.0 International License, which permits any non-commercial use, sharing, distribution and reproduction in any medium or format, as long as you give appropriate credit to the original author(s) and the source, provide a link to the Creative Commons licence, and indicate if you modified the licensed material. You do not have permission under this licence to share adapted material derived from this article or parts of it. The images or other third party material in this article are included in the article's Creative Commons licence, unless indicated otherwise in a credit line to the material. If material is not included in the article's Creative Commons licence and your intended use is not permitted by statutory regulation or exceeds the permitted use, you will need to obtain permission directly from the copyright holder. To view a copy of this licence, visit <http://creativecommons.org/licenses/by-nc-nd/4.0/>.

© The Author(s) 2024

Acknowledgements

This work was supported by a National Research Foundation of Korea (NRF) grant funded by the Korean government (MSIT) (NRF-2018R1A5A1024958). S.-I.A. was supported by the Yonsei Fellowship, funded by Lee Youn Jae. M.F.S. was supported by the NSF grant AGS-2141728. This is an IPRC publication 1626 and SOEST contribution 11859. J.-H. Park was supported by the National Research Foundation of Korea (NRF) grant funded by the